



Production of hydrogen by water photo-splitting over commercial and synthesised Au/TiO₂ catalysts

J.A. Ortega Méndez^{a,*}, Cristina R. López^a, E. Pulido Melián^a, O. González Díaz^{a,*}, J.M. Doña Rodríguez^a, D. Fernández Hevia^{a,c}, M. Macías^b

^a Centro Instrumental Físico-Químico para el desarrollo de Investigación Aplicada (CIDIA-FEAM), Departamento de Química, Universidad de Las Palmas de Gran Canaria, Edificio Polivalente I del Parque Científico Tecnológico, Campus de Tafira, 35017 Las Palmas de Gran Canaria, Spain

^b Instituto de Ciencia de Materiales de Sevilla, Centro Mixto CSIC-Universidad de Sevilla, Américo Vespucio s/n, 41092 Sevilla, Spain

^c INAIL Electrical Systems, C/Jarama 5, 45007 Toledo, Spain



ARTICLE INFO

Article history:

Received 11 July 2013

Received in revised form

16 September 2013

Accepted 19 September 2013

Available online 27 September 2013

Keywords:

Methanol

H₂ production

Photocatalysis

Photo-splitting

Au plasmon

ABSTRACT

H₂ production from methanol/water photo-splitting was compared using various commercial photocatalysts (Evonik P25 (P25), Hombikat UV-100 (HB) and Kronos vlp7000 (KR)) and others synthesised with a sol-gel-hydrothermal (HT) process and a sol-gel method followed by calcination (SG400 and SG750). All photocatalysts had been surface modified with Au at different concentrations, from 0.2 to 6.0 wt.%, using the photodeposition method. A complete characterisation study of the different photocatalysts was performed (BET, XRD, TEM, SEM-EDX, FTIR, UV-vis Reflectance Diffuse Spectra and aggregate size). The experiments were conducted for 3.5 h using 1 g L⁻¹ of photocatalyst with methanol (25 vol.%) as sacrificial agent. In addition to H₂ generation, production of the main intermediates, formaldehyde and formic acid, and of CO₂ was also evaluated. The commercial photocatalyst KR at 0.8 wt.% Au had the highest H₂ production of all the photocatalysts studied with 1542.9 μmol h⁻¹. Of the photocatalysts synthesised by our group, SG750 at Au loading of 2.0 wt.% gave the highest H₂ production of 723.1 μmol h⁻¹. The SG750 photocatalyst at Au loading of 2.0 wt.% also had the highest H₂ production yield per unit of surface area at 45.5 μmol g⁻¹ m⁻².

© 2013 Published by Elsevier B.V.

1. Introduction

In recent years a significant number of studies have involved the search for clean energy sources [1,2]. There is an evident need for an alternative energy source that can at least partially and progressively replace fossil fuels in the near future. Though it is not devoid of complications, hydrogen is beginning to be seen as the most viable and advantageous option of the various clean energy sources available as an energy vector. The benefits of using H₂ as an energy source do not lie solely in its being a virtually inexhaustible raw material whose heat of combustion with oxygen (14.19×10^4 kJ kg⁻¹) is notably higher than that of classic fossil fuels such as, for example, gasoline ($\sim 4.5 \times 10^4$ kJ kg⁻¹). Importantly, its combustion does not produce CO₂, but exclusively water vapour.

Due to its low economic cost, there has been growing interest in the production of H₂ from water by photocatalysis (photo-splitting) through the use of semiconductors. A significant number

of research studies are being undertaken along these lines aimed at enhancing the efficiency of this process [1].

The main drawback of water-splitting by photocatalysis is the low levels of H₂ production as a result of the extremely rapid recombination of the electron-hole pair on the photocatalyst surface. One way of improving the efficiency of this process is based on the incorporation on the photocatalyst surface of noble metal nanoparticles and the presence of organic species like methanol as sacrificial agents which act as a hole scavenger much more efficiently than the water itself.

The use of methanol as sacrificial agent is an acceptable option given its high hydrogen/carbon ratio and the fact it contains no carbon–carbon links thus reducing the risk of carbon formation and so subsequent fouling of the photocatalyst [2].

When noble metal nanoparticles are deposited on the photocatalyst surface, the photopromoted electrons migrate preferentially from the conduction band of the semiconductor to the metal, resulting in a decrease in electron-hole pair recombination. The main reason for this behaviour is based on separation of the photogenerated charge carriers generally attributed to the formation of a Schottky barrier at the metal/TiO₂ interface. The higher the Schottky barrier, the lower the recombination rate between the electron transferred to the metal and the hole and the greater the production

* Corresponding authors. Tel.: +34 928457298; fax: +34 928457397.

E-mail addresses: jaortegamendez@gmail.com (J.A. Ortega Méndez), ogonzalez@dqui.ulpgc.es (O. González Díaz).

of H₂ [3]. To date, various metals have been used as co-catalyst on a titanium surface including, amongst others, Pt [4], Pd [5], Cu [6] and Au [7]. Of these, the best yields in terms of photocatalytic production of H₂ have been obtained with Pt/TiO₂ and Au/TiO₂ [8]. Additionally, in recent years use has been made of so-called bimetallic systems [9], such as Au–Pd [10] or Au–Pt [11], for the water-splitting reactions. The cooperative effect between these different metals helps to enhance catalytic performance.

In this context, gold is generally considered to be a catalyst of low activity. However, various studies [12] have found that when it is highly dispersed or as a reducible metal oxide, it displays high activity. The role of the metal oxide is to stabilise the gold nanoparticles and make the reaction take place on the gold surface. Though there is an ongoing debate as to the cause of this high activity of gold, it is accepted that ultimately it depends on particle size, support properties (semiconductor or insulating), preparation procedure and pre-treatment conditions of the photocatalyst [13].

In this study, photocatalytic activity for H₂ production was tested using various commercial photocatalysts (Evonik P25 (P25), Hombikat UV-100 (HB) and Kronos vlp7000 (KR)) and others synthesised with a sol–gel–hydrothermal process (HT) and a sol–gel method followed by calcination (SG400 and SG750). The methodology used in the preparation of the synthesised photocatalysts has been described in a previous study [14]. All photocatalysts were surface modified by photodeposition of Au particles and a comparison made of their activity in production of H₂. Analyses were conducted of photocatalytic activity, the presence of Au and of the different structural characteristics of the photocatalysts.

2. Experimental

2.1. Photocatalysts preparation

The photocatalysts were synthesised following a sol–gel procedure based on a previous work of the authors [14]. A mixture of ethanol and titanium tert-butoxide in molar relation 50:3.5 was released drop-by-drop onto an ethanol–water mixture with 9.83 × 10⁻² M citric acid. The suspension was then stirred for 30 min and kept in the dark for a period of 48 h. The photocatalyst was then dried at 105 °C for 24 h. After this ageing and drying treatment, the dry powder was sieved through a 63 µm mesh. As a final step, various batches were separated from the raw powder and subjected to 3.5 h of calcination at temperatures of 400 °C and 750 °C. A 0.5 °C min⁻¹ heating ramp was programmed accordingly. The resulting photocatalysts were designated SG400 and SG750, corresponding to the two calcination temperatures used. Another set of batches from the raw powder was subjected not to calcination but to a mild hydrothermal treatment at 150 °C for 24 h. The photocatalyst obtained in this way was designated HT.

A photodeposition method was used for Au loading on the surface of the different photocatalysts [15]. For this, a cylindrical batch photoreactor was prepared with a 400 W medium-pressure lamp of maximum wavelength of 365 nm in the interior of a quartz inner tube. A predetermined amount of HAuCl₄·3H₂O (99.9%) obtained from Sigma-Aldrich was added to a suspension of the photocatalyst in 400 mL of Milli-Q water (2 g L⁻¹) and 9.4 mL of isopropanol. This was illuminated for 6 h under constant stirring and nitrogen flushing. Finally, it was filtered using a 0.45 µm Millipore nitrocellulose filter, washed with Milli-Q water and finally oven dried at 105 °C for 24 h.

2.2. Characterisation of photocatalysts

BET surface area, pore volume and pore size measurements were carried out by N₂ adsorption at 77 K using a Micromeritics ASAP 2010 instrument.

XRD patterns were recorded on a Siemens D-501 diffractometer equipped with a Ni filter and graphite monochromator using Cu K α radiation ($\lambda = 1.5418 \text{ \AA}$) to determine phase composition of the samples. Crystal sizes were estimated from line broadening of the corresponding X-ray diffraction peaks using the Scherrer equation.

UV-vis spectra were recorded on a Varian Cary 5 spectrometer equipped with an integrating sphere using PTFE (poly-tetrafluoroethylene) as reference to study light absorption properties of the samples. Diffuse reflectance spectra were recorded and band-gaps were calculated by the Kubelka–Munk function, according to the Tandon–Gupta method [16].

The morphology of the samples was studied by transmission electron microscopy (TEM) using a Philips CM 200 instrument operating at 200 kV and a nominal structural resolution of ~0.25 nm. Field emission scanning electron microscopy (FESEM) images were obtained using a Hitachi S-4800 microscope equipped with an EDX analysing system.

FTIR experiments were performed with a Nicolet iS10 spectrophotometer and a DTGS detector was used. Operating parameters were: intervals of 4000–1000 cm⁻¹, a 4 cm⁻¹ resolution with 32 scans and a mirror velocity of 0.6329 cm s⁻¹. These analyses were carried out by placing films of the photocatalysts between two CaF₂ windows.

Size distribution of aggregates in aqueous suspension was analysed using a Mastersizer Hydro 2000 SM unit.

The apparent quantum efficiencies (QE) were measured under the same photocatalytic reaction condition. The QE was calculated according to Eq. (1) following Yu et al. [17]. An Ocean Optics HR2000 + spectrometer was used for the measurement of incident photons in the wavelength range of 300–400 nm.

$$\begin{aligned} \text{QE}(\%) &= \frac{\text{number of reacted electrons}}{\text{number of incident photons}} \times 100 \\ &= \frac{\text{number of evolved H}_2\text{ molecules} \times 2}{\text{number of incident photons}} \times 100 \end{aligned} \quad (1)$$

2.3. Photocatalytic tests

The light source was a set of 3 Solarium Philips HB175 lamps, each equipped with 4 15 W Philips CLEO fluorescent tubes. Emission spectrum was 300–400 nm with a maximum peak at 365 nm. The lamps were externally arranged around the reactor tube in such a way that incident photon flux was maximised. The photoreactor was an own design [18] with 75 mL of aqueous suspension containing 25 vol.% methanol in water and a photocatalyst concentration of 1 g L⁻¹. The pH value of the aqueous suspension was set to ≥ 5 by means of an NaOH or H₂SO₄ solution. The photoreactor was operated in continuous mode by using He as inert “dragging” gas (10 mL min⁻¹) at 1 bar and ambient temperature. This flow, controlled with mass-flow measurement systems, was used to displace the hydrogen produced by photo-splitting from the photoreactor headspace towards the GC measuring system. Hydrogen production was monitored for 3.5 h through analysis in a gas chromatograph (Agilent 490 Micro GC with two channels, 5A molecular sieve and PPQ (Pora PLOT Q) column) equipped with an injector that has built-in 10 µL sample loop and a TCD detector. Chromatography peak areas were converted into hydrogen flux measurements through a previously obtained calibration line, recorded under the same

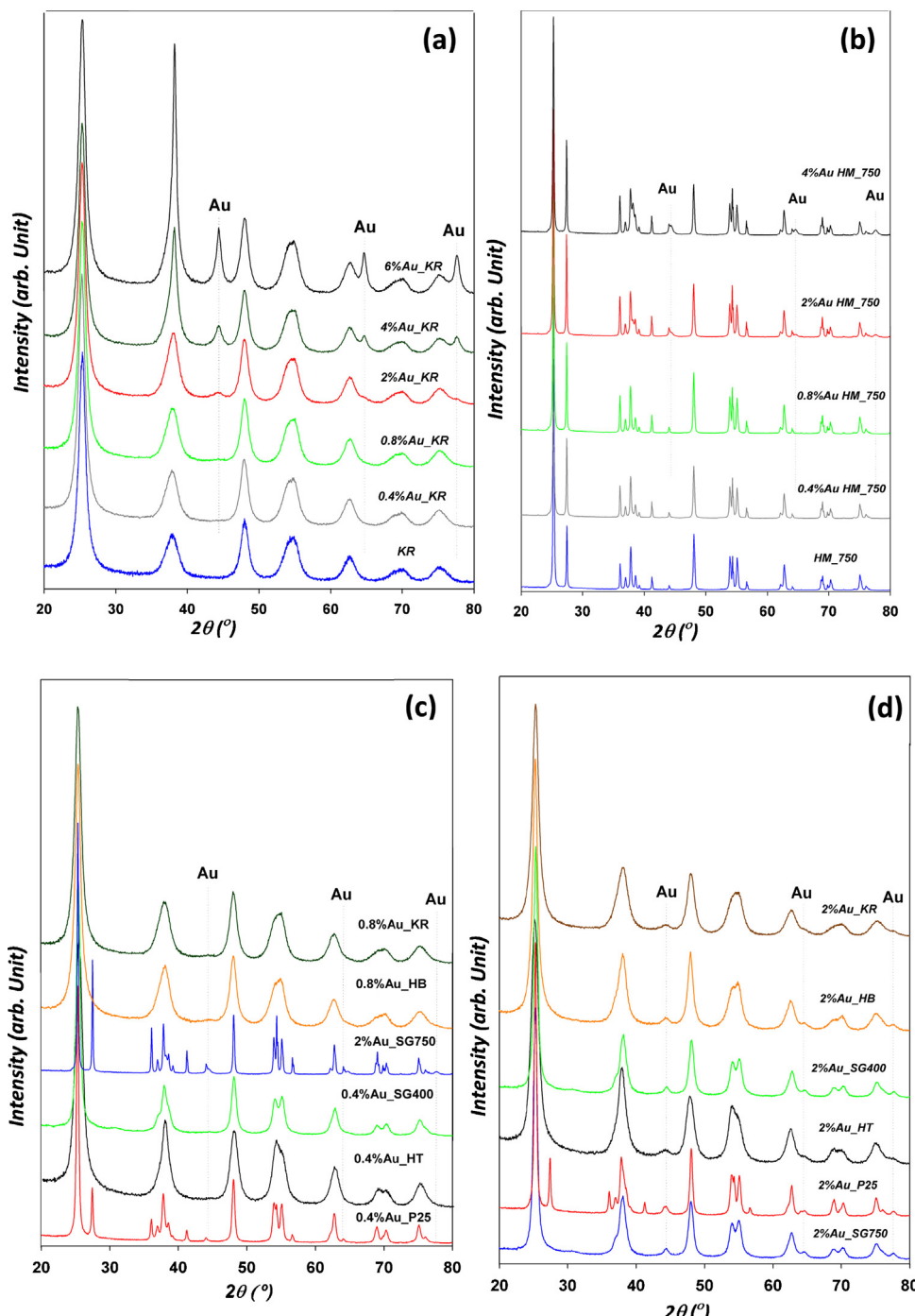


Fig. 1. XRD of the KR (a) and SG750 (b) photocatalysts for different photodeposited Au loadings. XRD of the photocatalysts with the highest production of H₂ (c) and of photocatalysts at 2.0 wt.% Au (d).

conditions. Final mineralisation degree and pH were measured by means of a Crison Basic20 pH-metre and a Shimadzu TOC-VCSN Total Organic Carbon analyser. Suspension concentrations of formaldehyde were quantitatively measured by spectrophotometry [19]. A Dionex ion-chromatography system (column: Ion PAC AS11-HC, mobile phase: 30 mM NaOH and suppressed conductivity ASRS-ULTRA) was used for the analysis of formic acid.

3. Results

3.1. BET and XRD analysis and pore volume distribution

Fig. 1 shows the XRD analyses performed on the KR (Fig. 1a) and SG750 (Fig. 1b) photocatalysts at the different photodeposited Au loading percentages. Notable for KR are the anatase peaks of $2\theta \cong 25.34^\circ$, 38.17° , 48.33° , 54.55° and 62.80° , corresponding to

Table 1

Structural characteristics of the commercial photocatalysts at different photodeposited Au loadings.

Catalyst	Band gap (eV)	Surface area ($\text{m}^2 \text{g}^{-1}$)	Content (%)		Crystal size (nm)		Pore volume ($\text{cm}^3 \text{g}^{-1}$)
			Anatase	Rutile	Anatase	Rutile	
HB	3.26	280	100	–	9.00	–	0.343
HB-0.4Au	3.22	302.8	100	–	8.79	–	0.337
HB-0.8Au	3.23	301.8	100	–	8.95	–	0.356
HB-2Au	3.19	245.1	100	–	10.45	–	0.362
KR	3.24	259	100	–	7.00	–	0.392
KR-0.4Au	3.20	290.8	100	–	8.02	–	0.413
KR-0.8Au	3.22	236.1	100	–	7.99	–	0.364
KR-2Au	3.14	263.7	100	–	8.03	–	0.392
KR-4Au	3.11	259.1	100	–	8.01	–	0.376
KR-6Au	3.06	297.3	100	–	8.07	–	0.434
P25	3.21	48.6	82.59	17.41	23.00	44.00	0.176
P25-0.2Au	2.90	47.9	82.46	17.54	23.47	34.39	0.39
P25-0.4Au	2.94	47.7	81.89	18.11	23.50	34.69	0.35
P25-0.8Au	2.95	48	80.35	19.65	23.42	33.30	0.4
P25-2Au	2.77	46.8	81.89	18.11	23.39	34.70	0.35

planes (1 0 1), (0 0 4), (2 0 0), (1 0 5) and (2 0 4), respectively [20]. For SG750, we also have the crystalline rutile phase peaks of $2\theta \approx 27.40^\circ$ and 30.06° , corresponding to planes (1 1 0) and (1 0 1), respectively.

From the XRD analyses it can be seen how the presence of Au on the photocatalyst surface through the photodeposition method does not result in any modification of the crystalline structure. Additional peaks to the catalyst are however observed which are attributed to the presence of surface-deposited Au⁰ [21]. The peaks correspond to the diffraction angles of $2\theta \approx 44.4^\circ$, 64.6° and 77.6° , which pertain to the planes Au (1 1 1), Au (2 0 0) and Au (2 2 0), respectively (JCPDS card No. 01-1174). It can be observed how the signal of the peak of Au is practically undetectable for the percentages with the highest production of H₂ (Fig. 1c) for the different photocatalysts. The signal of Au on the photocatalyst surface was only noticeable for concentrations of 2% and above of Au (Fig. 1d), with the clearest peak being $2\theta \approx 44.4^\circ$. At too low a concentration of Au (<0.8%), the peaks of gold are not clearly observable due to the weak signal which is below the detection limit of the instrument. According to some authors, XRD is unable to detect particles of reduced gold if their size is smaller than 5 nm [22].

BET surface area, pore volume and size and the percentages of anatase/rutile phases are shown in Tables 1 and 2 for both the commercial photocatalysts and those synthesised by our group and which displayed high activity in H₂ production in previous studies performed without photocatalyst modification [18]. In the present study, a comparison is made of the photocatalysts with and without different concentrations of Au photodeposition.

It can be seen in the tables how anatase content is not modified by the photodeposition process, though slight changes are observed in the SG750 series. One explanation for these variations could lie in the observations made in some studies [23] of how the Au nanoparticles could be facilitating the transition of anatase to rutile during the reduction of Au/TiO₂. The same authors also reported the existence of stronger rutile XRD reflections and a decrease in the anatase:rutile ratio as Au load rose. In the present study, as the Au percentage content rises, a small decrease of between 0.07 and 0.59 eV can be observed in the band-gap, depending on the photocatalyst. This fall is caused by the effect of Au plasmons and, consequently, by the shift of the absorption spectrum towards the visible region [24]. The band-gap decreases that were found are similar to those described by other authors with different photocatalysts and it would appear that this band-gap modification has no effect on the activity of the photocatalyst [24,25].

The photocatalysts with higher surface area are those whose structure is 100% anatase in the case of both the commercial and synthesised photocatalysts (though the surface area of SG400 is approximately 4 times lower than the other 100% anatase photocatalysts). Only the P25 and SG750 photocatalysts show rutile phase in their composition, with the latter of the two having the highest percentage at 27%.

In terms of surface area, no significant changes were observed in the photocatalysts synthesised by our group or the commercial photocatalyst P25 after photodeposition at the various Au percentage loadings. However, HB surface area rose at 0.2 wt.% Au and subsequently fell at higher Au loading percentages. As for

Table 2

Structural characteristics of the synthesised photocatalysts in their pure form and with different photodeposited Au loading percentages.

Catalyst	Band Gap (eV)	Surface area ($\text{m}^2 \text{g}^{-1}$)	Content (%)		Crystal size (nm)		Pore volume ($\text{cm}^3 \text{g}^{-1}$)
			Anatase	Rutile	Anatase	Rutile	
SG400	3.22	61.2	100	–	13.95	–	0.344
SG400-0.2Au	3.17	67.7	100	–	13.13	–	0.304
SG400-0.4Au	3.16	69.1	100	–	13.16	–	0.283
SG400-0.8Au	3.16	65.1	100	–	13.16	–	0.287
SG400-2Au	3.14	59.4	100	–	13.18	–	0.234
SG750	3.10	17.42	77.97	22.03	45.46	61.25	0.071
SG750-0.4Au	2.96	17.0	73.16	26.84	44.14	55.28	0.069
SG750-0.8Au	2.69	17.1	73.05	26.95	44.77	56.58	0.062
SG750-2Au	2.87	15.9	68.73	31.27	44.95	56.64	0.067
SG750-4Au	2.81	15.7	69.40	30.60	44.75	56.98	0.060
HT	3.11	224.2	100	–	7.43	–	0.206
HT-0.2Au	2.97	203.3	100	–	7.07	–	0.215
HT-0.4Au	2.87	161.2	100	–	7.03	–	0.131
HT-0.8Au	2.77	164.5	100	–	7.05	–	0.167
HT-2Au	2.52	169.5	100	–	7.02	–	0.173

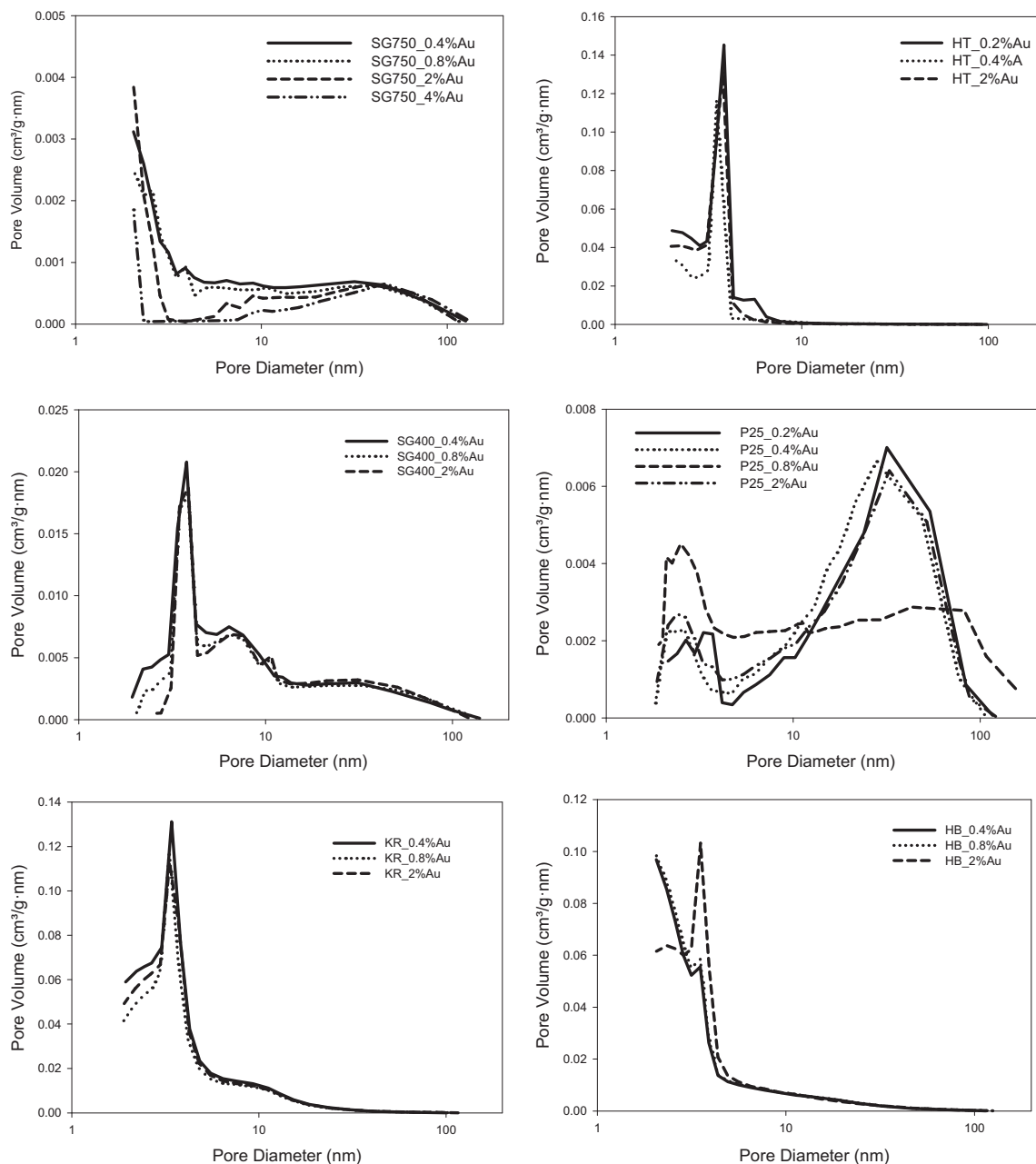


Fig. 2. Distribution of pore volume for the photocatalysts at different photodeposited Au loadings.

KR, its surface area rose and fell at the different photodeposited Au percentages. In terms of pore volume, SG750 is a non-porous photocatalyst with a practically constant and unvarying value of $0.0658 \pm 0.005 \text{ cm}^3 \text{ g}^{-1}$. With SG400 and HT a trend of a decrease in pore volume is observed, whereas for P25 the opposite trend is seen. For KR and HB pore volume also remains virtually unchanged. It should be noted that the decreases in surface area for SG400 and HT are accompanied by a decrease in pore volume. One explanation for the differences found in surface area and pore volume could lie in the difference in densities between the catalyst and the metal. In this respect, an increase in density of the Au/TiO₂ sample as metal load increases would result in a reduction in BET surface area and pore volume [26].

In relation to the above, Fig. 2 shows the pore volume distribution for the different photocatalysts. It can be seen how for the synthesised series there is practically no modification of pore volume distribution after the photodeposition process with Au, with

most probable pore size values of 2 nm for SG750 and 3.8 nm for HT and SG400. All pore volume distribution in these three cases is found in the region of low mesoporosity. The most significant changes are seen with P25, moving from the region of macroporosity at 0.2 and 0.4 wt.% Au to mesoporosity at 0.8 wt.% Au and returning again to macroporosity at 2.0 wt.% Au. This involves going from a most probable pore size of 31.49 nm to one of 2.45 nm before returning again to 31.49 nm. As for HB, and as can be seen from the values shown in Table 1, no modification in pore volume was observed. However, as can be seen in Fig. 2, a small modification was found for HB in pore size from 2 nm to around 3.5 nm at 2.0 wt.% Au.

The reduction in pore volume that was observed is caused by two related factors which have been commented on in other studies [26], namely the formation of smaller pores due to aggregation of Au nanoparticles and the incorporation of Au nanoparticles in the mesopores and macropores of the catalyst. Other authors [27,25]

have also referred to this phenomenon as a blocking of the pores of the catalyst by the Au nanoparticles.

3.2. DRS analysis

Fig. 3 shows the results of the UV-vis diffuse reflectance spectra for the different photocatalyst series at different Au loading. The band gaps of all samples were calculated according to the modified Kubelka–Munk function. A shift in all samples is observed of the absorption spectrum towards the visible light region with a broad band centred at around 550 nm, caused by the presence of gold nanoparticles in the photocatalyst matrix attributed to Au surface plasmon resonance, very similar to that found in other photocatalysts [25]. This band is most evident for the P25 and KR photocatalysts, and can also be seen for HT. There is a clear increase of this band even at 0.2 wt.% Au in both P25 and HT, though it is slightly less obvious in KR. For the HB, SG400 and SG750 photocatalysts, this shoulder at 550 nm is much less clear, with HB apparently the least affected by the presence of Au.

Some authors [28] suggest that these bands are the result of collective oscillations of free conduction-band electrons induced by interaction with incident electromagnetic radiation whose wavelength is much higher than the size of the particles. So, the position, intensity and shape of the plasmonic band seen in the spectra will depend on various factors including, amongst others, the size, shape and surface area of the Au nanoparticles [29], the Au loading and the electronic interaction of the gold nanoparticles with the photocatalyst. It has been proposed that especially gold nanoparticles of between 5 and 50 nm show a strong absorption band in the region of 520–530 nm. For particles larger than 50 nm, the absorption band widens to include the whole visible range, while for Au particles smaller than 5 nm, band intensity decreases and the band becomes almost flat for very small particles (<2 nm) [30].

3.3. TEM/SEM

Fig. 4 shows the TEM and SEM images taken of the different photocatalysts to observe the distribution of gold particles at 2.0 wt.% loading on the photocatalyst surface. Excellent gold particle dispersion can be observed for KR and SG750 as well as for HB and HT, all of which also display greater homogeneity in terms of particle distribution. Contrastingly for P25 and SG400, large-sized aggregates are found, principally in P25, and consequently a less homogeneous particle distribution. A bipyramidal, that is a more crystalline, appearance also seems to be apparent in both HT and SG, though further analyses are required at greater resolution to confirm it.

The above is more evident in the SEM images, which show especially for HB, HT and KR an excellent dispersion and distribution of the gold particles over the surface. The formation of large-sized Au aggregates is also clear for SG750.

Au particle size distribution is shown in **Fig. 5**. It can be observed how the series of commercial photocatalysts appears to display a more heterogeneous and wide-ranging distribution of sizes. However, particles smaller than 10 nm predominate with the synthesised photocatalysts SG750 and HT, while an Au particle size of around 20 nm is more prevalent for SG400.

It should be remembered that in order to favour the approach of the Au particles to the photocatalyst surface, the photodeposition process was performed at acid pH values below 5. At these pH values we have a positively charged TiO₂ surface leading to a strong interaction between the catalyst and gold particles and, consequently, a higher Au loading. The opposite would happen at high pH values [31,32]. This seems to concur with what is seen in both the TEM and SEM images for all the synthesised photocatalysts HT, SG400 and SG750, and for KR and HB of the commercial photocatalysts, but not for P25. In addition, **Fig. 5** shows a high

frequency of particle size above 25 nm for P25, which concurs with the large-sized aggregates observed in the TEM images. It should also be noted that Au particle size distribution should be generally symmetrical, regardless of the preparation method, as shown in other studies in which different methods have been used to support the Au particles [33].

3.4. Aggregate size

It can be verified how the presence of Au nanoparticles alters the aggregate size distribution of the original photocatalyst. **Fig. 6** shows how the synthesised photocatalysts SG400 and HT change from a unimodal to a bimodal distribution as the concentration of Au particles increases, with one peak below 10 μm and the other above 100 μm. However, SG750 is barely modified by the presence of Au particles on the surface, except for a slight shift towards lower-sized aggregates.

As for the commercial photocatalysts, it can be seen how KR remains practically unmodified by the effect of the presence of Au particles, while P25 displays a shift towards aggregate sizes around 100 μm after photodeposition.

In the case of HT, a change from a bimodal to trimodal distribution can be observed after photodeposition, with aggregate sizes with peaks around 1, 10 and 100 μm.

3.5. FTIR analysis

The FTIR spectra for the unmodified photocatalysts are shown in **Fig. 7I**. Bands are clearly visible at 3690 cm⁻¹ of the hydroxyl groups present on face (0 0 1) [34] of the P25 and SG400 photocatalysts, though this is much less evident in the other photocatalysts. A broad band is also observable between 3600 and 2500 cm⁻¹ which is attributed to bonded hydroxyl groups. This band can also be attributed to molecules of water adsorbed through hydrogen bonds or by Ti⁴⁺ atoms most probably to face (1 0 1) [35]. It can be seen how this band is slightly broader in the synthesised than the commercial photocatalysts. In the case of HT, a series of bands can also be seen at 1580 and 1403 cm⁻¹ [36] which are a product of the formation of formates and impurities as a result of the hydrothermal synthesis which were not eliminated at the temperatures which were used.

The FTIR spectra of the various photocatalysts with different Au percentages are shown in **Fig. 7II**. It can be seen how the amplitude of the band between 3600 and 2500 cm⁻¹ increases after the photodeposition process. This is due to hydration of the photocatalyst and so to the increase of absorbed water molecules [14]. Also noticeable is a higher intensity in the bands due to the isolated hydroxyl groups at 3690 cm⁻¹. This response is generally more evident at more acidic pH values [14], and it should be remembered that photodeposition is usually performed at acid pH values, so the effect commented on here may be due to the photodeposition process itself. This higher intensity is seen in turn in the band at 1627 cm⁻¹ for all the photocatalysts, caused by an increase in water physisorbed on the photocatalyst surface.

The FTIR spectra after the H₂ production assays of 3.5 h using methanol as sacrificial agent are shown in **Fig. 7III**. A stretching of the band at 1618 cm⁻¹ can be observed along with the appearance of a new band at 1421 cm⁻¹ [36] the product of the adsorption of formates resulting from the generation of formic acid in the medium during the reaction. This occurs principally in the commercial catalysts for which higher concentrations of this compound have been identified.

Also possible, as reported by other authors, is the presence on the photocatalyst surface of methoxy species [14,37] whose bands are usually found at 2923, 2814, 1125 and 1055 cm⁻¹, though these generally overlap with the bands of the formates. There is also the

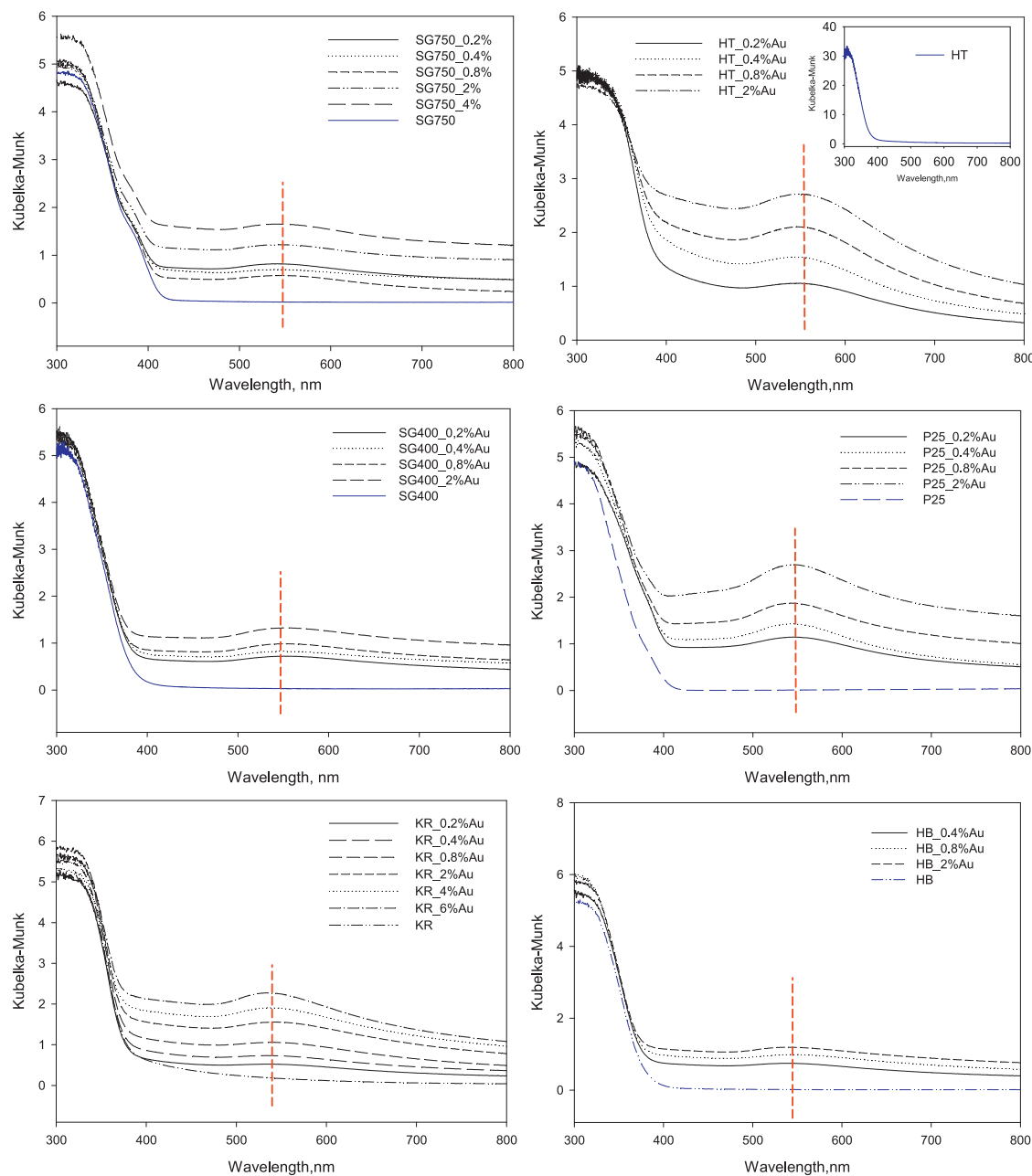


Fig. 3. Diffuse reflectance spectra for the different photocatalysts and their respective photodeposited Au loadings.

possibility of the presence of formaldehyde on the photocatalyst surface. These bands usually appear with a shoulder at 1596 cm^{-1} , together with bands at 2731 and 2844 cm^{-1} , and this is usually ascribed to formaldehyde adsorbed on gold [37]. Bearing in mind the concentrations of this compound (see Fig. 9), found especially on the commercial photocatalysts, the bands that appear in the spectra at 1568 cm^{-1} for P25, KR and HB, can be attributed to its presence.

3.6. Hydrogen production

Fig. 8 shows the results of H_2 production for the various commercial and synthesised photocatalysts at the different photodeposited Au loadings. All the assays were performed in triplicate, with the mean and standard deviation being shown (see Table 3). It can be seen how, of the commercial photocatalysts, KR stands out in terms of H_2 production in all the studied photodeposited

Au levels with a maximum production of $1542.9\text{ }\mu\text{mol}$ (17.55% QE) in 3.5 h at 0.8 wt.\% Au . KR was followed by HB whose maximum production of H_2 also took place at 0.8 wt.\% Au with $818.75\text{ }\mu\text{mol}$ (9.31% QE). The lowest H_2 production by the commercial photocatalysts was in P25 with a maximum production at 0.4 wt.\% Au of $363.9\text{ }\mu\text{mol}$ (4.14% QE), though a very similar value of $352.68\text{ }\mu\text{mol}$ (4.01% QE) was observed at 0.8 wt.\% Au . Maximum production of H_2 for the commercial photocatalysts therefore took place at 0.8 wt.\% Au . However, the highest activity shown by the synthesised photocatalysts was with SG750 at 2.0 wt.\% Au with a value of $723.1\text{ }\mu\text{mol}$ (8.22% QE) of H_2 after 3.5 h . Maximum production with SG400 and HT was obtained at 0.4 wt.\% Au with 522.52 and $512.85\text{ }\mu\text{mol}$ (5.94 and 5.83% QE), respectively. For SG400 and SG750, production of H_2 ranged between 453.6 and $522.5\text{ }\mu\text{mol}$ and between 302.9 and $723.12\text{ }\mu\text{mol}$, respectively. For the commercial photocatalysts P25 and HB, production values ranged between 268.8 and $363.9\text{ }\mu\text{mol}$, and between 700.9 and $818.7\text{ }\mu\text{mol}$, respectively.

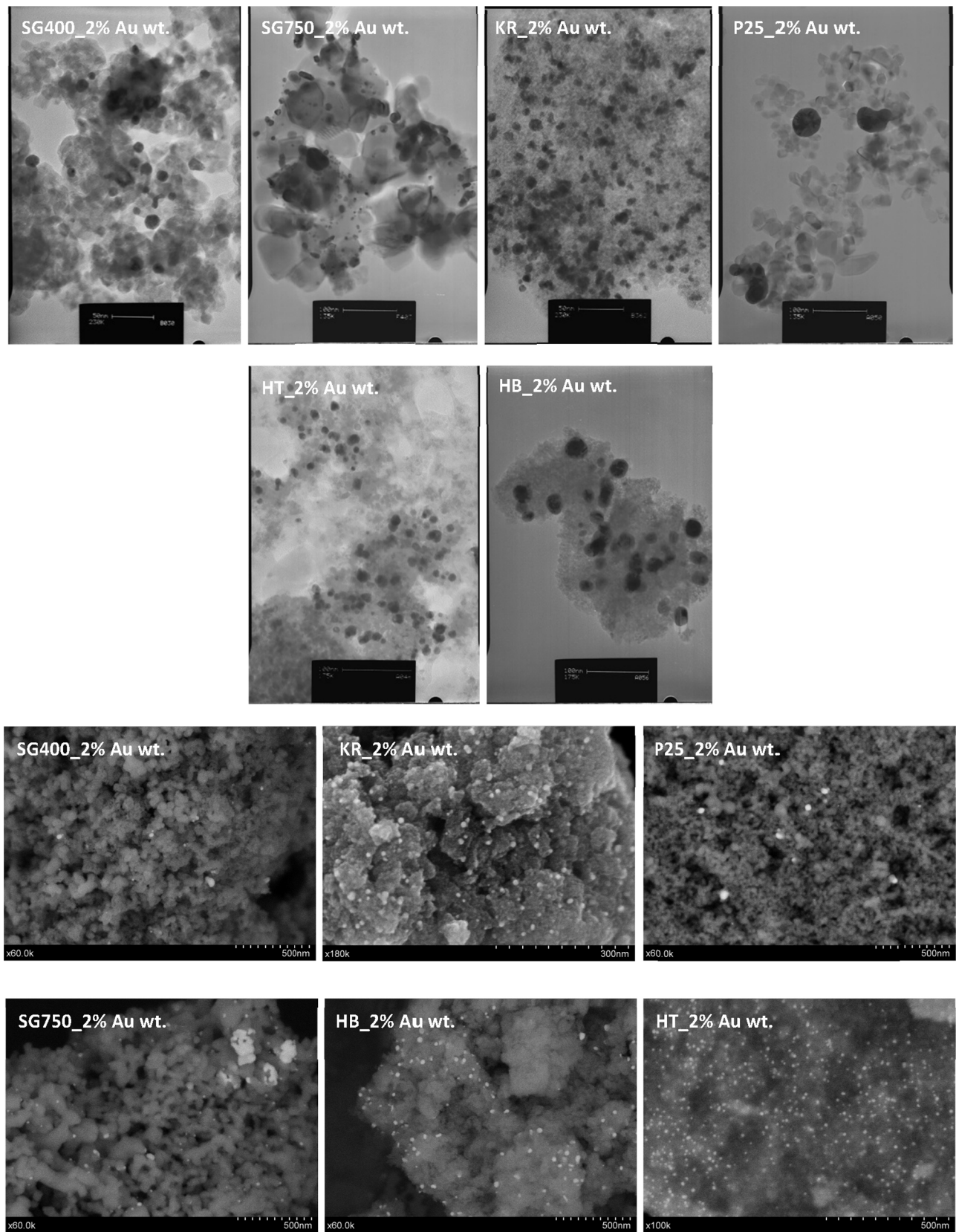


Fig. 4. TEM/SEM images of the photocatalysts at 2.0 wt.% photodeposited Au loading.

When estimating the production of H₂ in terms of the surface areas obtained for the different photocatalysts, significant data were obtained. Fig. 8C shows clearly how SG750 has the highest activity per unit of surface area at all the studied percentages of

photodeposited Au, with production values that range between 17.8 and 45.5 $\mu\text{mol H}_2 \text{ g}^{-1} \text{ m}^{-2}$ and a maximum production at 2.0 wt.% Au. The other photocatalysts display a relatively similar activity of little variation of between 3 and 7.8 $\mu\text{mol H}_2 \text{ g}^{-1} \text{ m}^{-2}$.

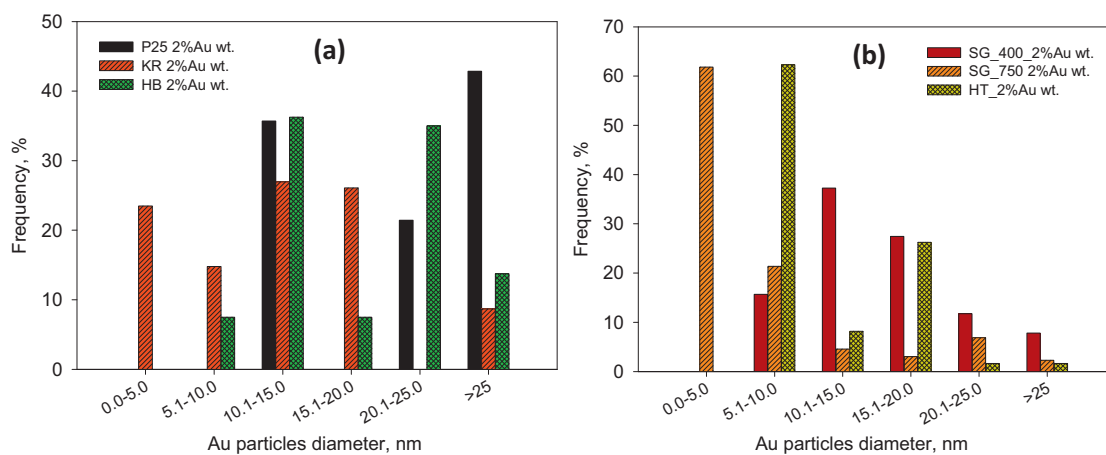


Fig. 5. Size distribution of Au particles at 2.0% loading on the surface of the commercial (a) and synthesised (b) photocatalysts.

That is, SG750 has values 6 orders of magnitude higher than the other photocatalysts in terms of production of H₂ per unit of surface area.

3.7. Production of intermediates

The main intermediates generated in the production reaction of H₂ from methanol are formaldehyde, formic acid and CO₂ [28,38]. Fig. 9 shows how formaldehyde is the most generated main intermediate for all the photocatalysts. In the case of KR, a decrease in formaldehyde concentration can be observed as Au loading increases, with a maximum concentration of 1038 ppm at 0.2 wt.% Au. For the other commercial photocatalysts, the production of formaldehyde is very similar at all Au loadings and ranges between 183 and 293 ppm. For its part, formic acid is found in lower concentrations but it is significant that the behaviour of its production is similar to that of H₂ production. Maximum production of formic acid at 547 ppm is found for KR at 0.8 wt.% Au, coinciding with the maximum production of H₂. A lower maximum formic acid production of 75.5 ppm is found for P25 at 0.4 wt.% Au, though this also coincides with its maximum H₂ production. For HB, formic acid concentration decreases as photodeposited Au loading increases, with a maximum concentration of 285 ppm at 0.4 wt.% Au, which in this case does not coincide with maximum H₂ production.

Formaldehyde concentration for the synthesised catalysts was very similar to that for HB and P25. The highest concentration was found for SG750 at 2.0 wt.% Au with 436.5 ppm. For SG400 and HT, maximum values were obtained of 306.6 ppm and 313.6 ppm, respectively, at 0.4 wt.% Au in both cases. These maximum values

coincide with the maximum H₂ production for the different photocatalysts. Maximum concentration values were obtained for formic acid of 184.9 for SG400 at 0.8 wt.% Au, 88.7 for SG750 at 2.0 wt.% Au and 32.6 ppm for HT at 0.2 wt.% Au.

As for CO₂ generation, the results in Fig. 10 show how the CO₂ is formed in similar concentrations for the commercial and synthesised photocatalysts. P25 generated the highest concentrations of all the photocatalysts at 0.4 and 0.8 wt.% Au. For KR, there is a very similar distribution to that obtained in H₂ production and in the formation of the different intermediates. In the case of HB, the increase in CO₂ concentration coincides with the increase in Au loading.

It can be seen for all the synthesised photocatalysts how maximum CO₂ production takes place at 2.0 wt.% Au. In the case of SG750, maximum CO₂ generation coincides with maximum H₂ production. However, as with HB, for SG400 CO₂ concentration increases with the Au loading percentage.

In general, we know that the methanol reforming reaction takes place in two stages involving the two main intermediates, formaldehyde and formic acid, and finally the CO₂:



According to different authors [39], reaction (4), involved in the formation of CO₂, is highly influenced by the pH value of the solution. HCOOH easily dissociates into H⁺ and HCOO⁻. At acid pH

Table 3

Summary of the results obtained in the hydrogen production with different synthesised and commercial catalysts.

Synthesised				Commercial			
Catalysts	Au loading (%)	H ₂ ± Sd (μmol h ⁻¹)	QE (%)	Catalysts	Au loading (%)	H ₂ ± Sd (μmol h ⁻¹)	QE (%)
SG750	0.4	302.977 ± 8.456	3.45 ± 0.10	Kronos	0.2	991.555 ± 4.821	11.28 ± 0.05
SG750	0.8	326.287 ± 4.062	3.71 ± 0.05	Kronos	0.4	1220.513 ± 11.765	13.88 ± 0.13
SG750	2	723.122 ± 12.248	8.22 ± 0.14	Kronos	0.8	1542.935 ± 11.754	17.55 ± 0.13
SG750	4	595.719 ± 17.663	6.78 ± 0.20	Kronos	2	1082.047 ± 11.754	12.31 ± 0.13
SG400	0.2	453.609 ± 4.357	5.16 ± 0.05	Kronos	4	985.976 ± 5.163	11.21 ± 0.06
SG400	0.4	522.529 ± 5.421	5.94 ± 0.06	Kronos	6	892.6632 ± 4.098	10.15 ± 0.05
SG400	0.8	462.051 ± 4.777	5.26 ± 0.05	P25	0.2	341.662 ± 6.695	3.89 ± 0.08
SG400	2	464.945 ± 5.935	5.29 ± 0.07	P25	0.4	363.901 ± 7.094	4.14 ± 0.08
HT	0.2	375.5271 ± 6.743	4.27 ± 0.08	P25	0.8	352.681 ± 4.260	4.01 ± 0.05
HT	0.4	512.849 ± 2.603	5.83 ± 0.03	P25	2	268.766 ± 8.392	3.06 ± 0.10
HT	0.8	450.419 ± 2.494	5.12 ± 0.03	Hombikat	0.4	777.582 ± 3.127	8.84 ± 0.04
HT	2	431.105 ± 1.868	4.90 ± 0.02	Hombikat	0.8	818.752 ± 8.176	9.31 ± 0.09
				Hombikat	2	700.946 ± 8.453	7.97 ± 0.10

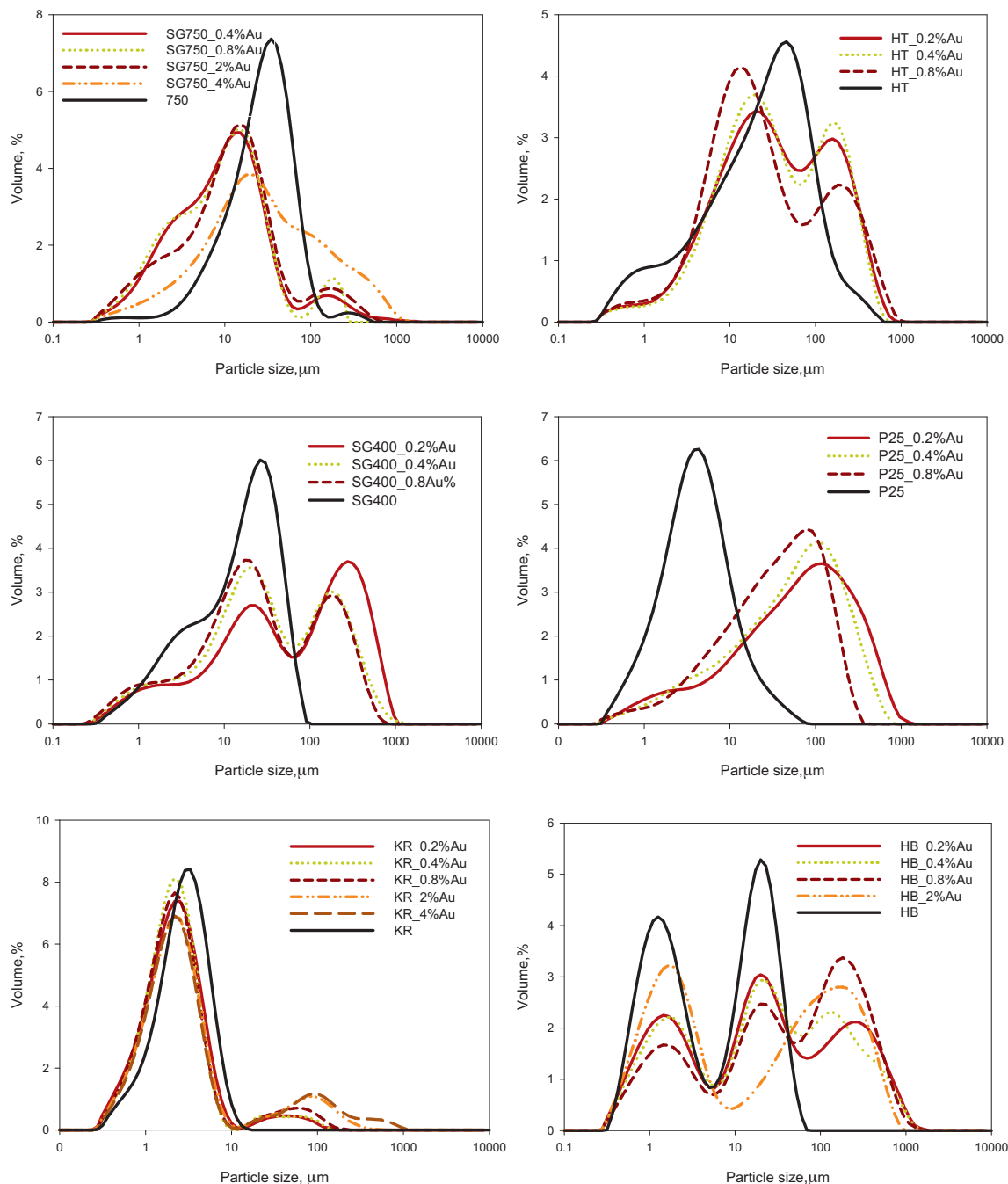


Fig. 6. Distribution of particle aggregates.

values, formic acid can be suppressed and this would be seen in a low production of H₂. However, at high pH values, formic acid is more easily oxidised to form CO₂ due to its deprotonation [40]. All the assays performed commenced with pH values of 5.04 ± 0.05 and terminated with a final slightly acidic pH value of 4.55 ± 0.34, which could be one of the possible explanations for the low production of CO₂ by the catalysts.

Carbon monoxide is another possible decomposition by-product, produced principally as the result of formic acid dehydration, but in this study no CO was detected [38].

4. Discussion

Comparing the results of this study with those of previous studies using photocatalysts without photodeposited Au

particles [18], an increase is observed of up to two orders of magnitude in terms of H₂ production. One possible explanation may be the important role played by the gold nanoparticles on the electron sinks, slowing down or impeding recombination of the electron–hole pairs, as well as offering new active sites which would entail a substantial increase in H₂ production yield [41].

In view of the results, the maximum production for the different photocatalysts which was obtained follows the general relationship detailed below (optimum Au percentage between parentheses):

$$\text{KR}(0.8\%) > \text{HB}(0.8\%) > \text{SG750}(2\%) > \text{SG400}(0.4\%) > \text{HT}(0.4\%) \\ > \text{P25}(0.4\%)$$

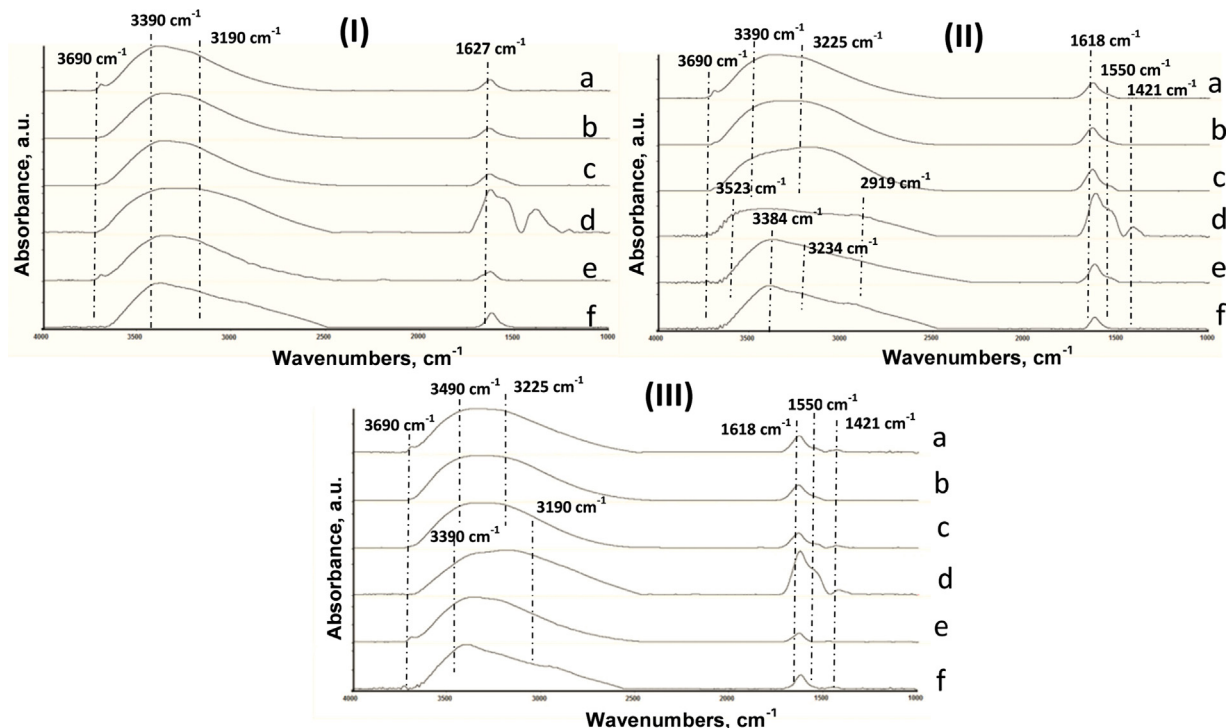


Fig. 7. (I) FTIR spectra of unmodified catalysts (a) P25, (b) HB, (c) KR, (d) HT, (e) SG400, (f) SG750. (II) FTIR spectra of photodeposited catalysts (a) P25_0.8%Au, (b) HB_0.4%Au, (c) KR_0.8%Au, (d) HT_0.4%Au, (e) SG400_0.4%Au, and (f) SG750_2%Au. (III) FTIR spectra of catalysts after the assays (3.5 h) (a) P25_0.8%Au, (b) HB_0.4%Au, (c) KR_0.8%Au, (d) HT_0.4%Au, (e) SG400_0.4%Au, and (f) SG750_2%Au.

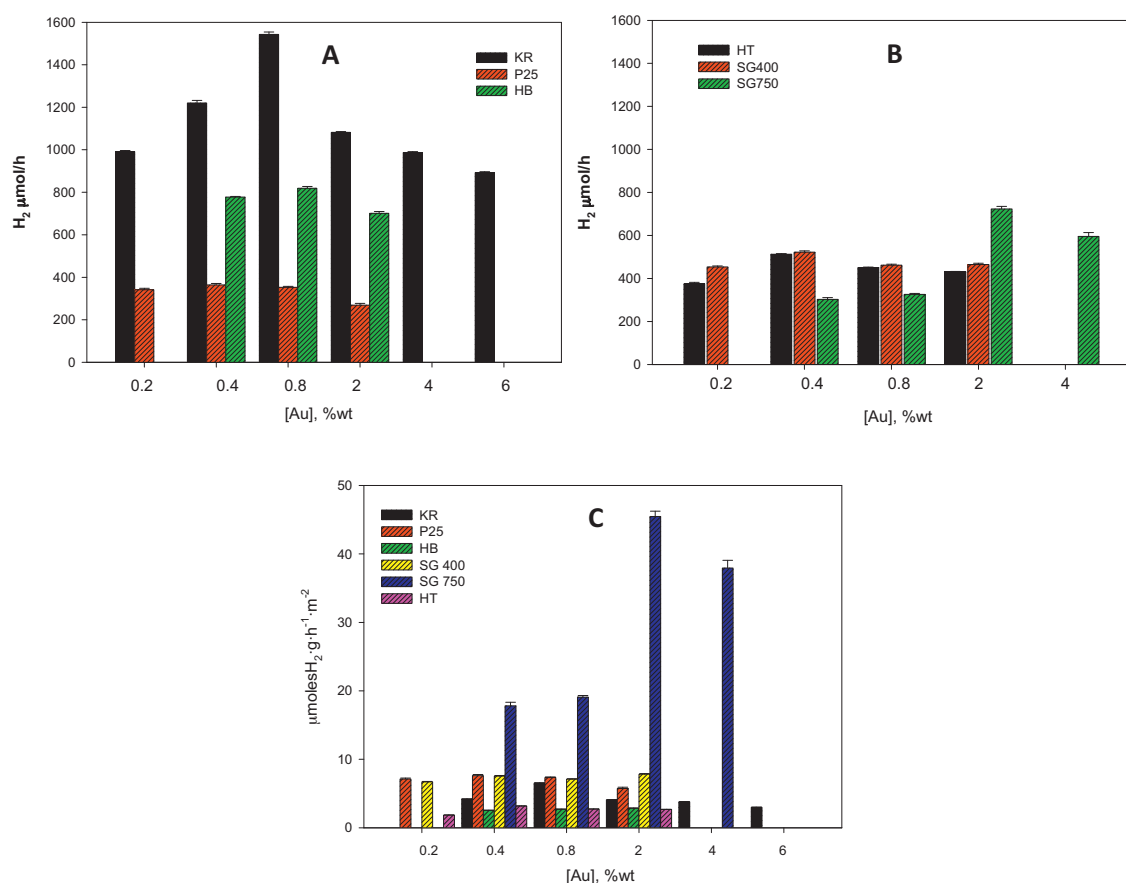


Fig. 8. Production of H₂ for the commercial (A) and synthesised (B) catalysts and production of H₂ per unit of surface area for all the catalysts (C).

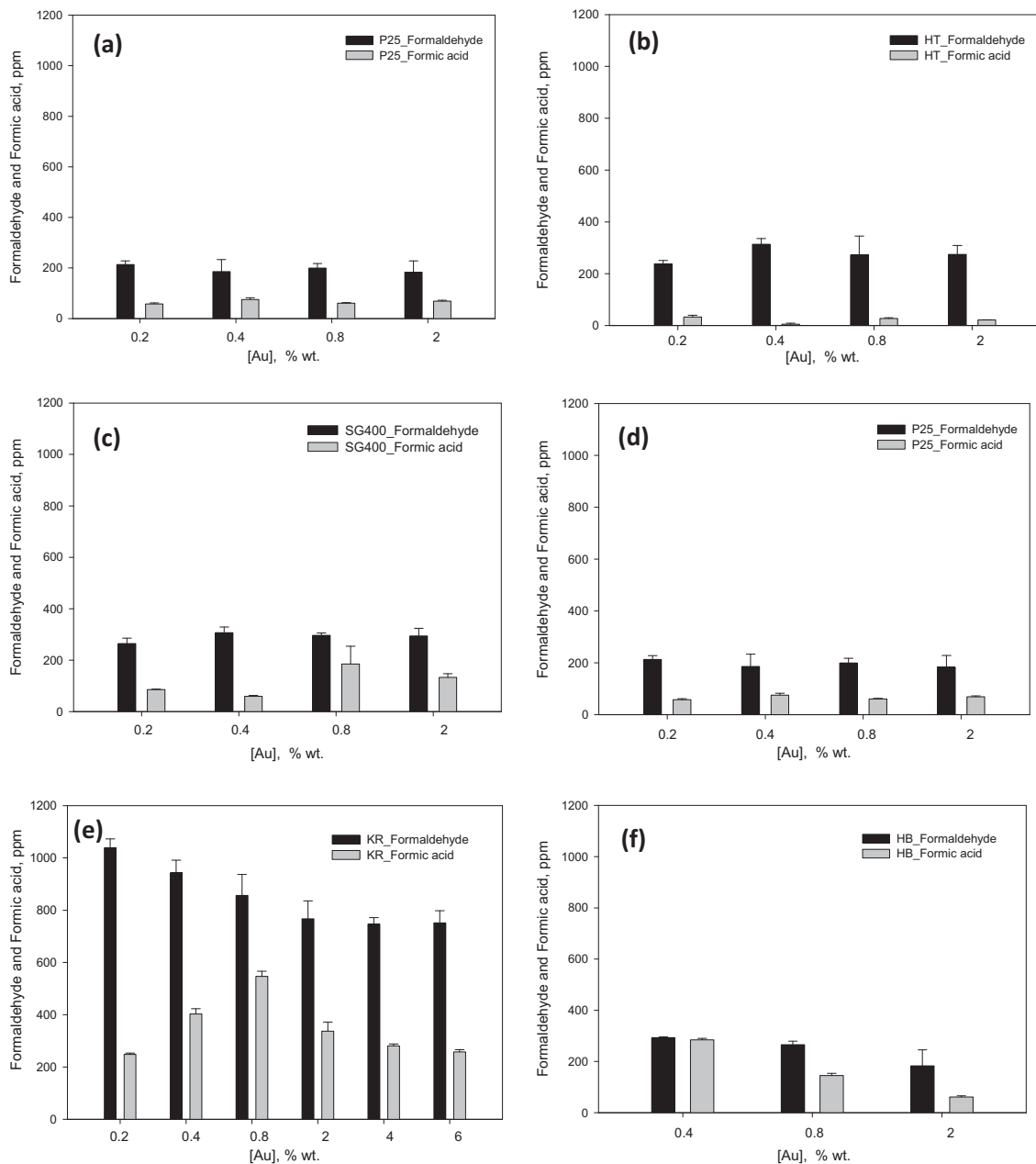


Fig. 9. Production of the intermediates formaldehyde ■ and formic acid □ for the photocatalysts SG750 (a), HT (b), SG400 (c), P25 (d), KR (e) and HB (f).

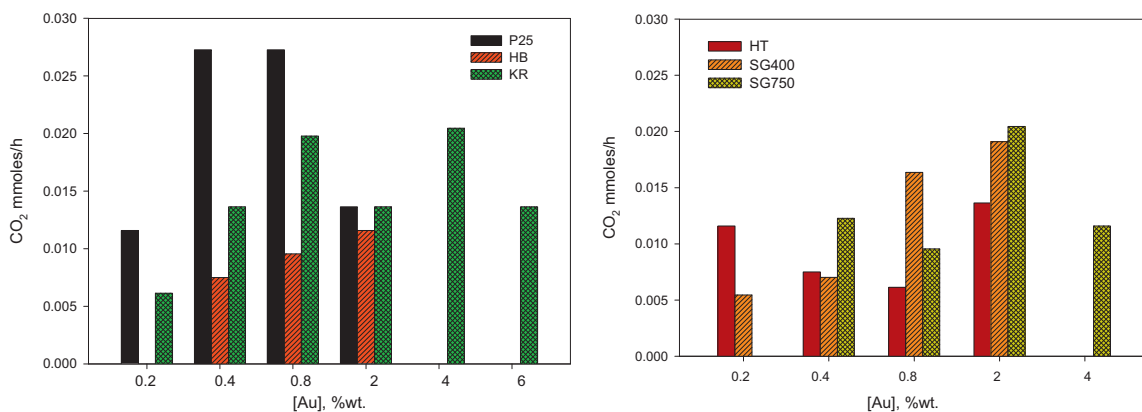


Fig. 10. Ratio of CO₂ from the assays with different catalysts at pH 5, MeOH at 25% (V=75 mL) with 1 g L⁻¹ catalyst, 3.5 h of reaction.

The results show how the production of H₂ by the different photocatalysts improves at higher photodeposited Au percentage loadings. For all the commercial (*P25, KR and HB*) and two of the synthesised (*SG400 and HT*) photocatalysts, optimum loading oscillates between 0.4 and 0.8 wt.% Au, while for *SG750* maximum production was obtained at 2.0 wt.% Au. This result for *SG750* is highly significant as it is the same optimum Au loading obtained in studies by other authors using different synthesised photocatalysts [24,33,42], though this is not necessarily always the sole optimum loading as it will depend on the test conditions and the sacrificial agent used in the reaction. Some observations can be made based on the results of the present study with respect to the role of Au in the production of H₂ for the different photocatalysts.

Some studies have been published [26,43], with similar results to those obtained in the present work, which may help shed light on the role played by the noble metal in the catalytic activity of the catalyst in hydrogen production. One of the main reasons for the reduction in activity in terms of hydrogen production at the highest Au percentage loadings may be the increase in opacity and consequent light dispersion. In this respect, it should be noted that darkening of the catalyst was observed as load percentage increased. This would entail a decrease in effective UV radiation falling on the catalyst. Other possible explanations that have been proposed [17,26] include partial blocking of surface active sites due to an excess of metal or deterioration of the catalytic properties of metal nanoparticles due to their enlargement. Another possibility [25] is that excess gold nanoparticles in the nanocomposites could act as the recombination centre of photo-generated charges to reduce photocatalytic activity in H₂ production, as observed in the tests with high Au loads.

Many authors have attempted to find some relationship between H₂ production and the different structural characteristics of the various photocatalysts used. In this sense, it is important to highlight, amongst other factors, the importance of the method used to obtain the photocatalyst and the Au particle support [33], the size of the Au particles [44], the anatase/rutile ratio [24], crystalline phase and size of the TiO₂ particles [42].

The first parameter to analyse is based on the surface area of both the photocatalyst and the Au particles. The order in terms of surface area of the photocatalyst with Au is as follows: *KR* ≈ *HB* > *HT* > *SG400* > *P25* > *SG750*. In this case, it would be expected that the higher the surface area the higher the number of active centres available for Au particle anchoring, which would in turn mean higher production of H₂. This relationship is met in the case of *KR* and *HB*, but not for the remaining photocatalysts. The other factor that could affect H₂ production is the surface area of the Au particles. In this case, previous studies [33] by other authors have shown that this characteristic is not directly linked to H₂ production, though they propose that it could play an important role in the photoredox processes between the interface of the TiO₂ and the Au particles themselves. Along these lines, it is known that it is important for the particles to be widely dispersed over the surface or as reducible metal oxide for high activity to take place [12]. In the present study, the TEM/SEM images displayed a high degree of Au particle dispersion for *KR, HB, SG750* and *HT*, though it was not as high for *SG400* and *P25* which additionally displayed large-sized aggregates.

Another line of investigation developed by some authors [39] is the direct relationship between gold particle size and H₂ production. They place emphasis on the migration of photogenerated electrons from the semiconductor to the Au not taking place until the two Fermi levels are aligned. On the other hand, the Schottky barrier [3] formed between the Au particles and the TiO₂ interface can serve to prevent electron-hole recombination in the photocatalysis. In this context it has been commented that small gold particles can induce a much higher negative change of the Fermi

level compared to larger sized particles [45]. This change is an indication of a larger charge separation and improved reduction potential for the photocatalyst. So, the photocatalyst with smaller sized articles will be much more catalytically active than that with larger sized particles. At the metal-TiO₂ interface, ions of metals with a higher work function than that of TiO₂ increase the Schottky barrier effect which helps to lower electron-hole recombination. So, metals with a suitable work function can help electron transfer, leading to higher photocatalytic activity, and also overcome the Schottky energy barrier. The work function of Au is 5.1 eV which is higher than that of TiO₂ (4.2 eV) favouring the catalytic reaction [45,46].

As seen in Fig. 8, the highest production yields of H₂ were obtained with photocatalysts with a higher concentration of particles of a size below 5 nm. The clearest example of this is the *SG750* at 2.0 wt.% Au, which has a high concentration of particles in this range compared to the other photocatalysts.

As for the other structural characteristics which may improve the activity of the photocatalysts, the structure of the TiO₂ and the crystalline phase, the results show how the predominance of anatase phase could favour higher activity in terms of production of H₂. One of the reasons could be that the anatase phase has a higher energy level for the conduction band (-0.20 V vs. NHE) than the rutile phase (0.04 V), so the electrons in the conduction band could more easily contribute to the reduction reaction as has been reported in other studies [47,48]. In this context, it should be noted that the photocatalysts with highest H₂ production in this study were *KR* and *HB*, both 100% anatase, though production was less in the cases of *HT* and *SG400*, both also 100% anatase. Both *SG750* and *P25* have a mixed anatase/rutile phase, and the first of these obtained a higher H₂ production than either *HT* or *SG400*, though at a higher Au loading of 2.0 wt.%.

On the other hand, various authors [14,47,48] have found that both anatase and rutile crystals, of large size and small surface area, display high activity, and not only for the production of H₂. The main reason is that the electrons in the conduction band of the larger-sized titanium dioxide particles whose active centres have a long life have more possibility of interacting with the compound, slowing down the electron-hole recombination rate and thereby enhancing catalytic reaction. The largest sized TiO₂ particles in the present study were for *SG750*, followed by *P25*, while the smallest sized particles were for *KR* and *HB*.

In general, it can be seen how the photocatalysts with 100% anatase composition (*KR, HB, HT* and *SG400*) give the best results in terms of H₂ production at low Au concentrations. In the mixed phase photocatalysts, the size of the crystals of the anatase/rutile phases could be a factor [47,48] affecting H₂ production at low Au percentages, with *SG750* having larger sized crystals and higher activity than *P25*. At higher percentages of photodeposited Au, *SG750* activity was even higher than of *HT* and *SG400* with 100% anatase phase. In this respect, the size of the Au particles, less than 5 nm as observed for *SG750*, was a determining factor for higher activity in terms of H₂ production.

It is more complicated to obtain a direct relationship between the production of the different intermediates and H₂ generation. In the synthesised photocatalysts it has been seen how maximum H₂ production coincided with maximum formaldehyde formation, but this relationship does not hold for the commercial photocatalysts. The opposite relationship occurs in the case of formic acid. Remembering that the formic acid concentrations were lower than those of formaldehyde, the maximum H₂ production yields for the synthesised photocatalysts coincided with the lowest formation of formic acid. One possible reason put forward by some authors [49] for the low levels of formic acid formation is the low density of the electron states in the proximity of the Fermi level of the noble metals. In the Au particles, the d-bands are at much

lower energy levels, so the Fermi energy density is much lower. This would mean that formic acid formation would be kinetically impeded by the Au particles, which would explain the low levels of formic acid generation in the tests. Nonetheless, the most unusual case in terms of formic acid is seen with the KR photocatalyst, with both formic acid and H₂ production displaying very similar behaviour.

5. Conclusions

The production of H₂ using Au photodeposited photocatalysts showed a high level of activity of up to 2 orders of magnitude greater than the results obtained from studies using pure photocatalysts. Highest H₂ production was recorded for the KR photocatalyst throughout the range of Au percentages. This could be due to various reasons, including its 100% anatase composition, large surface area, small-sized gold particles and their homogenous distribution on the photocatalyst surface. Of the photocatalysts with anatase/rutile phase the highest H₂ production of 723.1 μmol was obtained with the synthesised photocatalyst SG750 at 2.0 wt.% Au. This production was higher than with the commercial photocatalyst P25 throughout its range of Au photodeposition. In this case, the size of both the crystals of the crystalline phases and of the Au particles was of fundamental importance. This can be seen in the case of SG750 which, at high Au loading and with a particle size lower than 5 nm, displayed higher activity than HT and SG400 and similar levels of activity to HB and KR at the same photodeposited Au percentages. The main intermediates of methanol degradation found were formaldehyde and formic acid and, to a lesser extent, CO₂. The low formation of both formic acid and CO₂ could be related to the use of an acidic pH and kinetic impedance caused by the Au particles.

Acknowledgements

We are grateful for the funding of the Spanish Ministry of Science and Innovation for their financial support through the Project GESHTOS (IPT-120000-2010-033). Cristina R. López also acknowledges the support of the FPI Grant Program of the Ministry of Education and Science. Finally, we would like to thank the Ministry of Economy and Competitiveness (MINECO) of the Government of Spain for their infrastructure support of the 2010 proposal UNLP10-3E-726.

References

- [1] G.L. Chiarello, D. Ferri, E. Sellì, *J. Catal.* 280 (2011) 168–177.
- [2] R. Meng Ni, M.K.H. Leung, D.Y.C. Leung, K. Sumathy, *Renew. Sust. Energy Rev.* 11 (2007) 401–425.
- [3] S.-K. Leea, C.-M. Zetterling, M. Östling, I. Åberg, M.H. Magnusson, K. Deppert, L.-E. Wernersson, L. Samuelson, A. Litwinc, *Solid State Electron.* 46 (2002) 1433–1440.
- [4] J. Chen, D.F. Ollis, W.H. Rulkens, H. Bruning, *Water Res.* 33 (1999) 669–676.
- [5] A. Dickinson, D. James, N. Perkins, T. Cassidy, M. Bowker, *J. Mol. Catal. A* 146 (1999) 211–221.
- [6] N.L. Wu, M.S. Lee, *Int. J. Hydrogen Energy* 29 (2004) 1601–1605.
- [7] M. Bowker, L. Millard, J. Greaves, D. James, J. Soares, *Gold Bull.* 37 (2004) 170–173.
- [8] A. Naldoni, M. D'Arienzo, M. Altomare, M. Marelli, R. Scotti, F. Morazzoni, E. Sellì, V. Dal Santo, *Appl. Catal. B* 130–131 (2013) 239–324.
- [9] V. Dal Santo, A. Gallo, A. Naldoni, M. Guidotti, R. Psaro, *Catal. Today* 197 (2012) 190–205.
- [10] Y. Mizukoshi, K. Sato, T.J. Konno, N. Masahashi, *Appl. Catal. B* 94 (2010) 248–253.
- [11] A. Gallo, M. Marelli, R. Psaro, V. Gombac, T. Montini, P. Fornasiero, R. Pievo, V. Dal Santo, *Green Chem.* 14 (2012) 330–333.
- [12] M. Haruta, S. Tsubota, T. Kobayashi, H. Kageyama, M.J. Genet, B. Delmon, *J. Catal.* 144 (1993) 175.
- [13] M. Valden, S. Pak, X. Lai, D.W. Goodman, *Catal. Lett.* 56 (1998) 7–10.
- [14] J. Araña, J.M. Doña-Rodríguez, D. Portillo-Carrizo, C. Fernández-Rodríguez, J. Pérez-Peña, O. González Díaz, J.A. Navío, M. Macías, *Appl. Catal. B* 100 (2010) 346–354.
- [15] M. Maicu, M.C. Hidalgo, G. Colón, J.A. Navío, *J. Photochem. Photobiol. A: Chem.* 217 (2011) 275–283.
- [16] S.P. Tandon, J.P. Gupta, *Phys. Status Solidi* 38 (1970) 363–367.
- [17] J. Yu, Y. Hai, B. Cheng, *J. Phys. Chem. C* 115 (2011) 4953–4958.
- [18] E. Pulido Melián, O. González Díaz, A. Ortega Méndez, C.R. López, M. Nereida Suárez, J.M. Doña Rodríguez, J.A. Navío, D. Fernández Hevia, J. Pérez Peña, *Int. J. Hydrogen Energy* 38 (2013) 2144–2155.
- [19] E.R. Kennedy, Formaldehyde: method 3500, in: NIOSH Manual of Analytical Method (NMAM), 4th ed., Atlanta, Issue 2, pp. 2–5.
- [20] Y.-F. Yang, P. Sangeetha, Y.-W. Chen, *Int. J. Hydrogen Energy* 34 (2009) 8912–8920.
- [21] T.-C. Ou, F.-W. Chang, L. Selva Roselin, *J. Mol. Catal. A: Chem.* 293 (2008) 8–16.
- [22] C.K. Chang, Y.J. Chen, C. Yeh, *Appl. Catal. A* 174 (1998) 13.
- [23] F. Cárdenas-Lizana, S. Gómez-Quero, H. Idriss, M.A. Keane, *J. Catal.* 268 (2009) 223–234.
- [24] O. Rosseler, M.V. Shankar, M.K.-L. Du, L. Schmidlin, N. Keller, V. Keller, *J. Catal.* 269 (2010) 179–190.
- [25] J. Fang, S.-W. Cao, Z. Wang, M. Mehdi Shahjamali, S.C.J. Loo, J. Barber, C. Xue, *Int. J. Hydrogen Energy* 37 (2012) 17853–17861.
- [26] J. Yu, L. Qi, M. Jaroniec, *J. Phys. Chem. C* 114 (2010) 13118–13125.
- [27] S. Zhu, S. Liang, Q. Gu, L. Xie, J. Wang, Z. Ding, P. Liu, *Appl. Catal. B* 119–120 (2012) 146–155.
- [28] G.L. Chiarello, D. Ferri, E. Sellì, *Catal. Today* 144 (2009) 69–74.
- [29] U. Kreibig, L. Genzel, *Surf. Sci.* 156 (1985) 678.
- [30] M.M. Alvarez, J.T. Khouri, T.G. Schaaff, M.N. Shafigullin, I. Vezmar, R.L. Whetten, *J. Phys. Chem. B* 101 (1997) 3706.
- [31] S. Ivanova, C. Petit, V. Pitchon, *Appl. Catal. A* 267 (2004) 191.
- [32] G.R. Bamwenda, S. Tsubota, T. Nakamura, M. Haruta, *J. Photochem. Photobiol. A* 89 (1995) 177.
- [33] G.R. Bamwenda, S. Tsubota, T. Nakamura, M. asatake Haruta, *J. Photochem. Photobiol. A: Chem.* 89 (1995) 177–189.
- [34] G. Munuera, F. Moreno, F. Gonzalez, J.S. Anderson, M.W. Roberts, F.S. Stone (Eds.), *Reactivity of Solids*, Chapman Hall, London, 1972.
- [35] S. Dzwigaj, C. Arrouvel, M. Breysse, C. Geantet, S. Inoue, H. Toulhoat, P. Raybaud, *J. Catal.* 236 (2005) 245–250.
- [36] Q. Gu, X. Fu, X. Wang, S. Chen, D.Y.C. Leung, X. Xie, *Appl. Catal. B* 106 (2011) 689–696.
- [37] M. Manzoli, A. Chiorino, F. Bocuzzi, *Appl. Catal. B* 57 (2004) 201–209.
- [38] G. Luca Chiarello, M.H. Aguirre, E. Sellì, *J. Catal.* 273 (2010) 182–190.
- [39] G. Wu, T. Chen, W. Su, G. Zhou, X. Zong, Z. Lei, C. Li, *Int. J. Hydrogen Energy* 33 (2008) 1243–1251.
- [40] M. Bideau, B. Claudel, L. Faure, H. Kazouan, *J. Photochem. Photobiol. A* 61 (1991) 269–280.
- [41] J.-J. Jiun-Jen Chen, J.C.S. Wu, P.C. Wu, D.P. Tsai, *J. Phys. Chem. C* 115 (2011) 210–216.
- [42] H. Yuzawa, T. Yoshida, H. Yoshida, *Appl. Catal. B* 115–116 (2012) 294–302.
- [43] Q. Xiang, J. Yu, M. Jaroniec, *J. Am. Chem. Soc.* 134 (2012) 6575–6578.
- [44] K. Kähler, M.C. Holz, M. Rohe, A.C. van Veen, M. Muhler, *J. Catal.* 299 (2013) 162–170.
- [45] V. Subramanian, E.E. Wolf, P.V. Kamat, *J. Am. Chem. Soc.* 126 (2004) 4943–4950.
- [46] P. Gomathisankar, D. Yamamoto, H. Katsumata, T. Suzuki, S. Kaneko, *Int. J. Hydrogen Energy* 38 (2013) 5517–5524.
- [47] L. Du, A. Furube, K. Yamamoto, K. Hara, R. Katoh, M. Tachiya, *J. Phys. Chem. C* 113 (2009) 6454–6462.
- [48] E. Kowalska, O.O.P. Mahaney, R. Abe, B. Ohtani, *Phys. Chem. Chem. Phys.* 12 (2010) 2344–2355.
- [49] A.A. Ismail, D.W. Bahnemann, S.A. Al-Sayari, *Appl. Catal. A* 431–432 (2012) 62–68.